

Evidence for the origin of layered deposits in Candor Chasma, Mars, from mineral composition and hydrologic modeling

Scott Murchie,¹ Leah Roach,² Frank Seelos,¹ Ralph Milliken,³ John Mustard,² Raymond Arvidson,⁴ Sandra Wiseman,⁴ Kimberly Lichtenberg,⁴ Jeffrey Andrews-Hanna,⁵ Janice Bishop,^{6,7} Jean-Pierre Bibring,⁸ Mario Parente,⁹ and Richard Morris¹⁰

Received 24 January 2009; revised 11 May 2009; accepted 10 June 2009; published 16 September 2009.

[1] New results from the Compact Reconnaissance Imaging Spectrometer for Mars and High Resolution Imaging Science Experiment and Context Imager cameras on Mars Reconnaissance Orbiter provide insights into the origin of interior layered deposits in Valles Marineris from analysis of a thick, well-exposed section in western Candor Chasma. Most of the deposit is dominated spectrally by nanophase ferric oxide like that found in the globally distributed eolian dust, with the addition of a prevalent component of monohydrated sulfates. A rippled mantle containing both pyroxene and monohydrated sulfate emanates from discrete layers, which are interpreted as interbedded basaltic sand. Ferric minerals are observed in most of the sulfate-rich layers, and locally a coarse-grained grayer component has been concentrated from the layers by sorting. Polyhydrated sulfates are concentrated in discrete layers high in the section, implying chasma-scale changes in brine chemistry during formation of the layered deposits. Hydrological models were constructed in order to assess whether evaporite deposition from groundwater discharge could have trapped eolian sediments to form the observed deposits. The predicted thickness and extent of the evaporite-trapped sediment is consistent with the distribution of interior layered deposits in Candor Chasma as well as in other chasmata of Valles Marineris. In this scenario, eolian dust and sand were trapped and lithified by evaporites formed by evaporation of groundwater discharge that was highly localized within the chasmata. Sulfates precipitated in the resulting saline conditions, and diagenetic alteration formed crystalline ferric minerals including hematite. This model links the layered deposits in Valles Marineris and those in Meridiani Planum to a common regional process.

Citation: Murchie, S., et al. (2009), Evidence for the origin of layered deposits in Candor Chasma, Mars, from mineral composition and hydrologic modeling, *J. Geophys. Res.*, 114, E00D05, doi:10.1029/2009JE003343.

1. Introduction

[2] Orbital mapping of the spectral signatures of aqueously formed minerals on Mars by Thermal Emission Spectrometer on Mars Global Surveyor (TES) [Christensen et al., 2001], Observatoire pour la Mineralogie, L'Eau, les

Glaces et l'Activité on Mars Express (OMEGA) [Bibring et al., 2005, 2006; Poulet et al., 2005; Gendrin et al., 2005a], and Compact Reconnaissance Imaging Spectrometer (CRISM) for Mars on the Mars Reconnaissance Orbiter [Murchie et al., 2007a; Mustard et al., 2008] provides a window into the record of near-surface liquid water throughout the planet's history. Alteration products formed in Mars' early to middle Noachian period are dominated by phyllosilicate with limited occurrences of carbonates, indicating alteration in an environment with a neutral to alkaline pH [Bibring et al., 2005, 2006; Poulet et al., 2005; Mustard et al., 2008; Ehlmann et al., 2008]. Aqueous minerals in younger Hesperian rocks are distinctly different and dominated by sulfate-rich assemblages with limited regional occurrences of rocks containing hydrated silica, both suggesting weathering under acidic conditions [Gendrin et al., 2005a; Mangold et al., 2008; Milliken et al., 2008]. The age dependence of the mineralogy of aqueous alteration products was recognized in OMEGA data [Bibring et al., 2006], and has persisted even as CRISM has detected greater diversity and a more widespread distribution of alteration products [Murchie et al., 2009a]. The major hypothesis to

¹Johns Hopkins University Applied Physics Laboratory, Laurel, Maryland, USA.

²Department of Geological Sciences, Brown University, Providence, Rhode Island, USA.

³NASA JPL, Pasadena, California, USA.

⁴Department of Earth and Planetary Sciences, Washington University, St. Louis, Missouri, USA.

⁵Department of Geophysics, Colorado School of Mines, Golden, Colorado, USA.

⁶SETI Institute, Mountain View, California, USA.

⁷NASA Ames Research Center, Mountain View, California, USA.

⁸Institut d'Astrophysique Spatiale, Orsay, France.

⁹Department of Electrical Engineering, Stanford University, Stanford, California, USA.

¹⁰NASA JSC, Houston, Texas, USA.

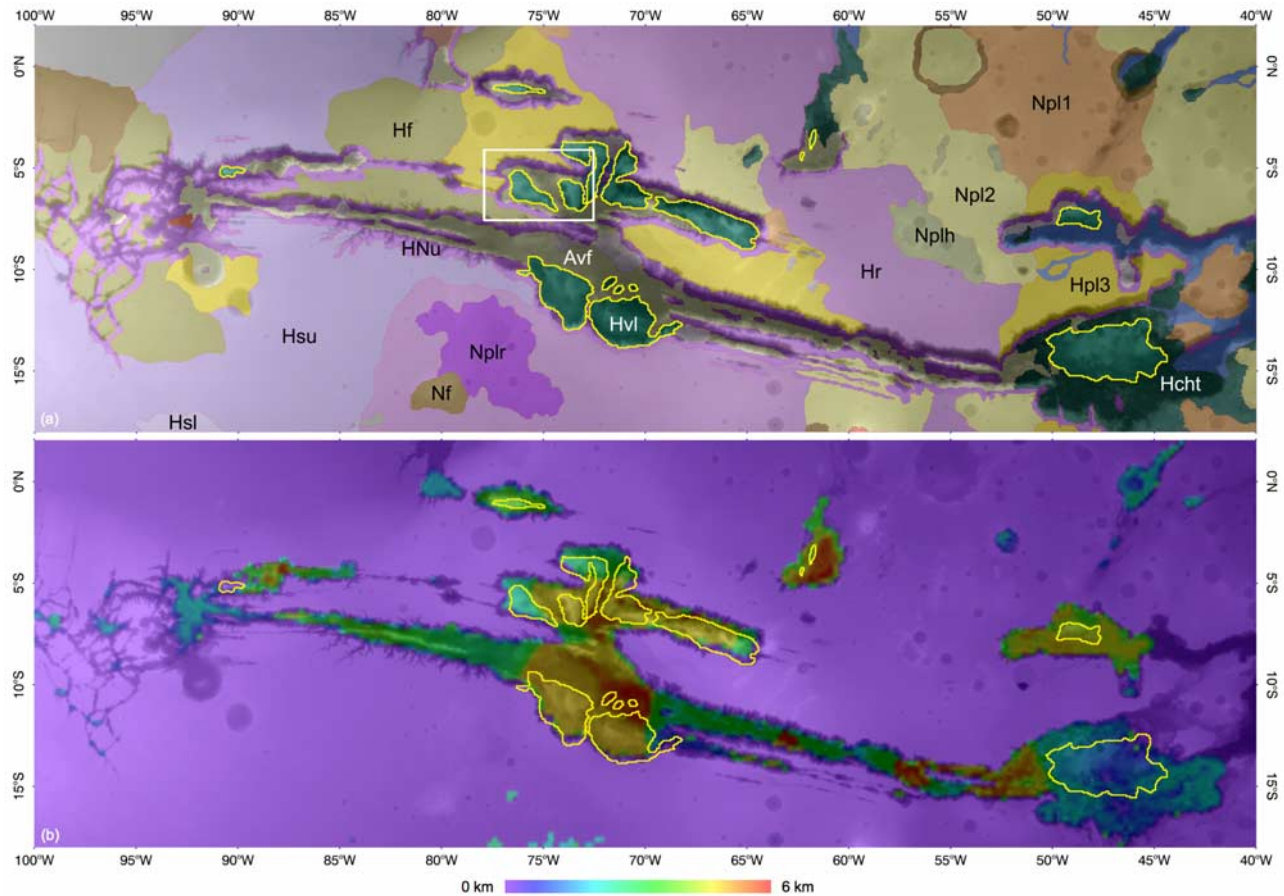


Figure 1. (a) Geologic unit map of the Valles Marineris region (adapted from *Scott and Tanaka [1986]*) overlain on a Mars Orbiter Laser Altimeter (MOLA) regional elevation map. The location of the study area in western Candor Chasma is outlined with the white box. Yellow lines are boundaries of the major occurrences of interior layered deposits. (b) Map of the predicted thickness of evaporite and trapped dust overlain on a MOLA regional elevation map. Yellow lines are boundaries of the major occurrences of interior layered deposits.

explain this change in Mars' alteration environment is that an early wet period during which phyllosilicates formed ended with the shutdown of Mars' dynamo and weakening of the magnetic field, which allowed solar wind to erode the early atmosphere, cooling and drying the climate. Contemporaneously, SO_2 emissions from construction of the Tharsis volcanoes provided a source of sulfur to acidify what liquid water occurred, leading to formation of sulfate-rich deposits [*Solomon et al., 2005*].

[3] The major occurrences of sulfate on Mars are in layered rocks in Meridiani Planum [*Arvidson et al., 2005*], Aram Chaos [*Glotch and Christensen, 2005*], and the interior layered deposits (ILDs) in the Valles Marineris chasma system [*Gendrin et al., 2005a; Mangold et al., 2008*]. Here we focus on the ILDs in Valles Marineris, particularly in Candor Chasma. Major aspects of the ILDs' composition were revealed by OMEGA and TES. OMEGA found that they are characterized by the presence of hydrated sulfate minerals and finely crystalline ferric oxides [*Gendrin et al., 2005a, 2005b; Bibring et al., 2007; Mangold et al., 2008*]. TES detected patches of coarser-grained, gray-colored hematite on and adjacent to the ILDs [*Christensen et al., 2001*].

[4] Two major questions about the Valles Marineris ILDs are their genetic mechanism, and their relationship to the sulfate- and hematite-bearing deposits elsewhere on the planet, especially in Meridiani Planum. From synthesis of orbital measurements by TES and OMEGA and landed measurements by the Mars Exploration Rover (MER) Opportunity [*Arvidson et al., 2006; Squyres et al., 2006*], the Meridiani deposits are interpreted to have formed where eolian sediments were trapped and ultimately lithified by sulfates deposited from the evaporation of upwelling groundwater, whose regional pattern of discharge was shaped by the late Noachian to early Hesperian formation of Tharsis [*Andrews-Hanna et al., 2007*]. As water rose through accumulated sediments, ferric iron was recrystallized into coarse-grained hematite. Later eolian erosion of the deposits exposed their internal layering and created lags of coarse-grained hematite.

[5] Here we report new constraints on the composition and stratigraphy of Valles Marineris' interior layered deposits provided by new results from CRISM [*Murchie et al., 2007a, 2009b*], the High Resolution Imaging Science Experiment (HiRISE) [*McEwen et al., 2007*], and the Context Imager (CTX) [*Malin et al., 2007*] on the Mars Reconnaissance

sance Orbiter. CRISM observations are at spatial resolution of up to 20 m/pixel and accompanying CTX and HiRISE images at 6 m/pixel and 0.3 m/pixel, respectively. We focus on western Candor Chasma, where a 5-km-thick accumulation occurs in the Candor Mensa and Ceti Mensa plateaus and is well exposed by heavy erosion, steep slopes, and a relative lack of dust cover (Figures 1a and 2). We show that the ILDs are dominated spectrally by materials consistent with dust and basaltic sand, both of which are accompanied by hydrated sulfates and one or more crystalline ferric minerals. We model the observed stratigraphy as a consequence of evaporation of saline groundwater discharge cementing and diagenetically modifying eolian sand, dust, and possibly volcanic ash. This model links interior layered deposits in Valles Marineris and the comparable deposits in Meridiani to a common, regional process.

2. Background

2.1. Geology of the ILDs

[6] The ILDs form eroded plateaus up to several kilometers in relief, whose major occurrences are on the floors of Tithonium, Hebes, Ophir, Candor, Melas, Eos, and Ganges Chasmata. The term “layered” is only loosely descriptive, because the morphological development of layers varies from chasma to chasma. Some parts of the deposits are highly deformed, as in southwestern Candor Chasma [Okubo *et al.*, 2008].

[7] The geology and geologic setting of the ILDs have been reviewed by Nedell *et al.* [1987] and Komatsu *et al.* [1993]. Their distribution and setting are summarized in the regional geologic map shown in Figure 1a, where the ILDs are outlined in yellow. Briefly, they are set on a deeply eroded basement consisting of the plateau plains series of Scott and Tanaka [1986] and Tanaka *et al.* [1992]. A series of Noachian (Npl₁ and Npl₂) and Hesperian (Hpl₃) plains units and their lateral equivalents deformed by fractures (Nf and Hf) or ridges (Nr and Hr) form the structure of the plateau plains. Where exposed in the chasma walls they are difficult to distinguish and are lumped into an undifferentiated unit (HNU); some hilly materials are mapped as unit Nh. The chasmata probably formed as fault-bounded grabens cutting these units, and the Hesperian-aged ILDs (mapped as unit Hvl) were superposed on the chasma walls and floors. Subsequently, large volumes of liquid water emanated from parts of the chasmata, eroding the ILDs. The topographically low regions between the remnant plateaus were partially infilled by Amazonian-aged valley floor material (unit Avf), interpreted as interlayered volcanic and fluvial and eolian sediments. Contemporaneously and later, the walls of the chasmata receded from the eroded plateaus of ILDs owing to faulting and landsliding.

[8] Proposed genetic mechanisms for the ILDs include subaerial fluvial deposition or volcanism [Lucchitta *et al.*, 1992], accumulation of eolian dust or sand [Peterson, 1981], evaporite precipitation [McKay and Nedell, 1988], or subaqueous volcanism [Nedell *et al.*, 1987]. Alternatively, Edgett and Malin [2003] argued that the ILDs are eroded remnants of preexisting layered chasma wall materials. Volumetric calculations suggest that the wall materials were only one of several sources of ILD material [Lucchitta *et al.*, 1994].

2.2. Composition of the ILDs

[9] The most detailed compositional study of ILDs in western Candor Chasma, by Mangold *et al.* [2008] using OMEGA data, showed that pyroxene is scarce and that the ILDs are characterized by widespread occurrence of hydrated sulfates. The dominant form of sulfates in the deposits is monohydrated, probably the Mg-rich phase kieserite. Monohydrate occurs predominantly on steep slopes, whereas polyhydrated sulfates are less common and occur on flatter slopes. The ILDs are draped by pyroxene-rich dunes which they interpreted to be derived from plateau plains materials exposed in the chasma walls. The presence of sulfates and the relative scarcity of pyroxene were interpreted to indicate a sedimentary origin for the deposits unrelated to formation of the chasma wall rocks. The polyhydrated sulfates were interpreted possibly to be a product of hydration of kieserite under modern ambient conditions as predicted by sulfate stability models [Vaniman *et al.*, 2004], or alternatively as an evaporite that formed near the same time as the kieserite.

[10] CRISM data cover ILDs in Candor and Juventae Chasmata and similar layered materials in Aram Chaos at up to twenty times the spatial resolution of OMEGA data and indicate a more complicated geologic history than was previously thought. In Juventae Chasma, polyhydrated sulfate overlies monohydrated sulfate and is separated by a distinct geologic contact. The shape and position of the 2.1- μm absorption due to monohydrated sulfate are most consistent with the Fe phase szomolnokite although lesser amounts of kieserite are also present [Bishop *et al.*, 2007, 2009]. In western Candor Chasma, the lower and middle parts of the section are dominated by monohydrated sulfate, which is most consistent with kieserite. However, as in Juventae Chasma, the upper beds are more dominated by polyhydrated sulfates [Murchie *et al.*, 2007b]. In Aram Chaos, the sequence of layered materials resembles that in ILDs in both Juventae and western Candor Chasmata, with polyhydrated sulfate overlying monohydrated sulfate resembling kieserite. However, unlike in the previous chasmata, the whole sequence is underlain by material having a spectral signature consistent with hydroxylated iron sulfate, possibly jarosite (K. Lichtenberg *et al.*, Stratigraphy of hydrated sulfates in the sedimentary deposits of Aram Chaos, Mars, submitted to *Journal of Geophysical Research*, 2009). Jarosite is known to be present in Meridiani Planum from MER Opportunity landed measurements [Klingelhöfer *et al.*, 2004], but the mineral is not detected in orbital spectral data [Arvidson *et al.*, 2006]. In eastern Candor Chasma, multiple layers of polyhydrated and monohydrated sulfates are intercalated, and the monohydrated phase is consistent with kieserite [Roach *et al.*, 2008, 2009]. The cooccurrence of sulfates in adjacent layers of the ILDs, their interbedding in eastern Candor Chasma, and the persistence of monohydrate on the several-year time scale of OMEGA and CRISM observations without alteration to polyhydrate indicate that monohydrate is not actively being altered to polyhydrated phases [Roach *et al.*, 2009]. Thus, exposures of different sulfates may represent different bedrock compositions, and convey information about their depositional and diagenetic environments.

[11] Ferric minerals including gray hematite [Christensen *et al.*, 2001] are associated with the sulfates in the Valles

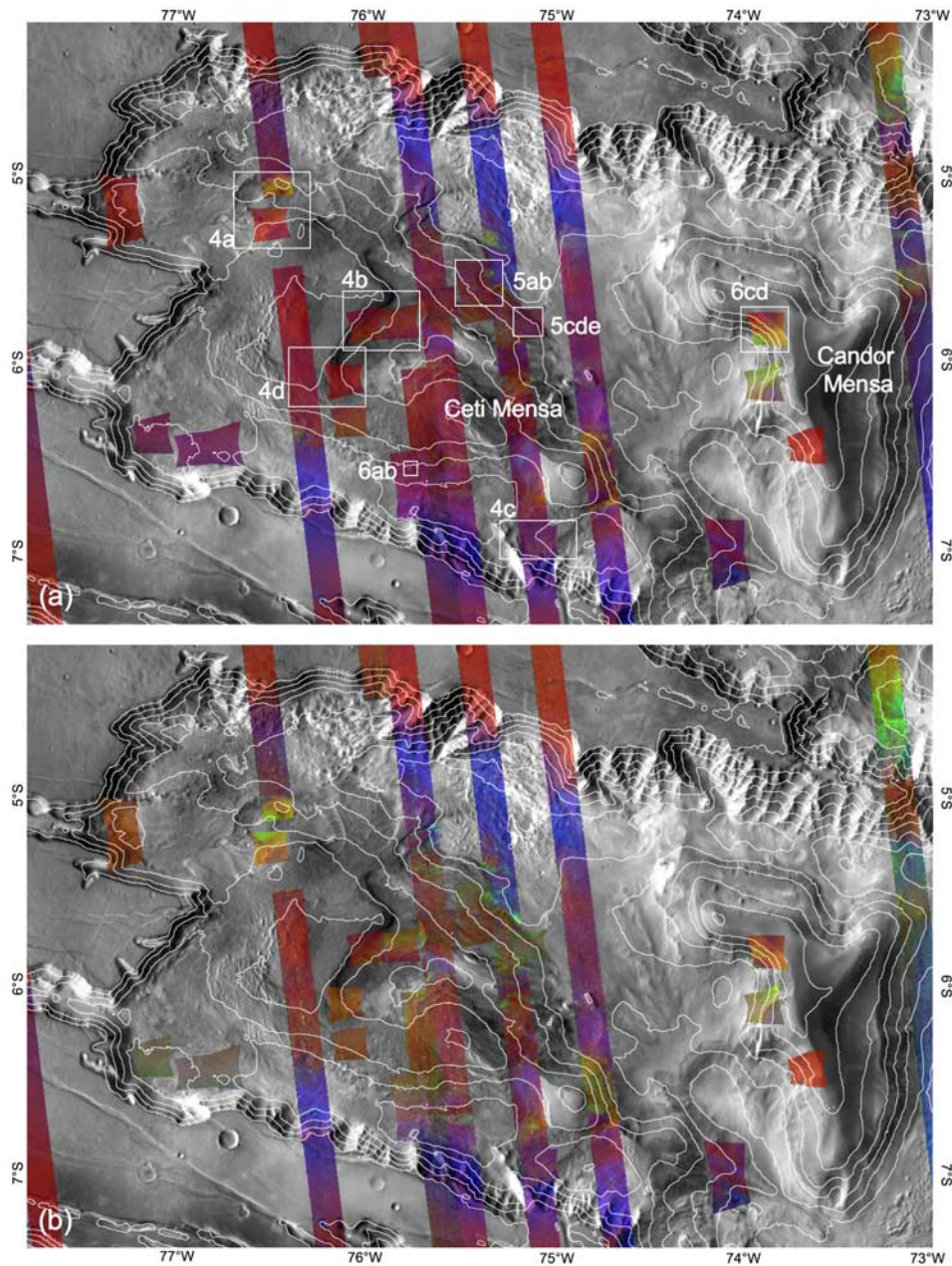


Figure 2. (a) Summary product versions of CRISM multispectral survey (long strips) and targeted (hourglass shaped) observations covering western Candor Chasma overlain on a THEMIS day IR mosaic. The white boxes show the locations of insets in Figures 4, 5, and 6. Elevation contours are shown in white at a 1-km interval. The red image plane represents depth of the $0.53\text{-}\mu\text{m}$ absorption in nanophase or finely crystalline ferric oxide (BD530); the green plane represents depth of the $0.9\text{-}\mu\text{m}$ absorption in crystalline ferric oxide (BD900); and the blue plane represents the integrated area in $1\text{-}\mu\text{m}$ absorption due to mafic minerals over the wavelength range $0.75\text{--}1.02\ \mu\text{m}$ (BDI1000VIS). The dynamic ranges of the red, green, and blue planes are 0.22, 0.03, and 0.02, respectively. (b) The red and blue image planes are the same as in Figure 2a, but the green plane is replaced with strength of the inflection in the spectrum due to the $2.4\text{-}\mu\text{m}$ band in hydrated sulfates (SINDEX). Dynamic range is 0.04.

Marineris ILDs and the Aram Chaos deposits. TES data [Christensen *et al.*, 2001] show that patches of gray hematite occur in close spatial association with the ILDs, typically at the base of slopes. The exact mineralogy of other ferric phases is uncertain. Higher spatial resolution data from OMEGA showed that finer-grained, red ferric minerals (possibly the oxide hematite) occur in the ILDs

and are concentrated in aprons around the eroded plateaus [Gendrin *et al.*, 2005b; Bibring *et al.*, 2007]. These observations were interpreted as evidence for their concentration by mass wasting [Gendrin *et al.*, 2005b; Mangold *et al.*, 2008]. Even higher spatial resolution data from CRISM show concentrations of ferric minerals not only in the aprons but also in dunes and patches scattered throughout

the ILDs. The materials typically have a red spectral slope from 1.0 to 1.8 μm characteristic of a number of ferric phases, but they vary in their infrared properties with some occurrences also exhibiting absorptions near 1.9 and 2.2 μm . Minerals that might explain these features include the hydrated ferric sulfate copiapite, the hydrated ferric oxyhydroxide ferrihydrite, or the oxide hematite in combination with one or more other hydrated sulfates [Roach *et al.*, 2007; Murchie *et al.*, 2007b; Bishop *et al.*, 2009].

2.3. Hydrologic Models of Layered Terrain Formation

[12] Interpreting the geologic history of layered materials in Meridiani Planum has greatly benefited from high spatial resolution ($5^\circ \times 5^\circ$ or better) hydrologic models of the recharge and discharge of groundwater. Andrews-Hanna *et al.* [2007] modeled the global precipitation-evaporation hydrologic cycle and incorporated regional topography. Precipitation is assumed to be distributed uniformly at latitudes equatorward of $\pm 45^\circ$ and to infiltrate a permeable surface. The water is assumed to leach subsurface rocks and accumulate salinity comparable to or in excess of that in terrestrial seawater. Subsurface flow is controlled by topography and an important effect is the development of Tharsis, which diverts existing subsurface water as well as recharge. Discharge occurs in topographically lower regions and in some regions with a topographic gradient, where the water table intersects the surface.

[13] The discharge is assumed to have promptly evaporated owing to arid conditions, depositing its dissolved load at or near the surface. Most discharge would have occurred in the northern plains, where its deposits would have been buried by later volcanics and sediments. A few regions predicted to have been sites of discharge remain exposed and are not superposed by younger geologic units; these include Meridiani Planum and other parts of Arabia, the interiors of the Hellas and Argyre basins, and Terra Sirenum near the southwestern flank of Tharsis. In Meridiani Planum, sulfate salts precipitated from the evaporating groundwater discharge are interpreted to have trapped and cemented eolian sediment, and driven diagenetic alteration to form the hematite concretions observed at the MER/Opportunity landing site [Squyres *et al.*, 2006; Arvidson *et al.*, 2006].

3. Data Reduction and Analysis

[14] CRISM data [Murchie *et al.*, 2007a, 2009b] were collected in two modes, multispectral mapping mode in 72 selected wavelengths at 200 m/pixel (5 times higher average spatial resolution than OMEGA), and targeted observations in 544 spectral bands with 6.55 nm sampling, at 18 m/pixel or 36 m/pixel when pixel binning was used onboard (10–20 times higher spatial resolution than OMEGA's highest resolution). CRISM's spectral range of 0.4–3.9 μm covers electronic transition absorptions due to olivine and pyroxene (dominant phases in Mars' basaltic crust) and their ferric alteration products [Adams, 1974; Cloutis and Gaffey, 1991; Sherman *et al.*, 1982; Sunshine *et al.*, 1990], and vibrational absorptions in H_2O -, hydroxyl-, and carbonate-bearing alteration products including phyllosilicates, sulfates, oxyhydroxides, and carbonates [Hunt and Salisbury, 1971a, 1971b; Rossman, 1976; Clark *et al.*, 1990; Cloutis *et*

al., 2006]. HiRISE acquired 30 cm/pixel images, 5 times higher resolution than MOC. The resulting 1-m spatial resolution is shown from terrestrial analog studies to resolve bed forms and structures diagnostic of important surface processes [McEwen *et al.*, 2007]. CRISM and HiRISE observations were typically coordinated with 6 m/pixel panchromatic images from the Context Imager (CTX) [Malin *et al.*, 2007] to provide local context.

[15] CRISM data shown in this paper were converted to apparent I/F using procedures described by Murchie *et al.* [2007a, 2009b]. Propagated detector noise was reduced using one of several filtering algorithms available [e.g., Parente, 2008]. Additional processing was used to correct for effects of illumination and atmospheric attenuation, to map project the data, and to highlight mineralogic variations. The data were divided by the cosine of the solar incidence angle and by a scaled atmospheric transmission spectrum obtained during an observation crossing Olympus Mons [Bibring *et al.*, 2005; Mustard *et al.*, 2008]. This corrects for atmospheric gases but not aerosols; to minimize effects of observations taken with high atmospheric opacities, we disregarded observations taken during the 2007 global dust event. All data were map projected using the line of sight intercept of each detector element with the Mars Orbiter Laser Altimeter (MOLA) shape model of Mars. To show variations in key mineralogic absorptions in image form, we use spectral parameters or “summary products” [Pelkey *et al.*, 2007], which are standardized representations of absorption band depths using wavelengths included in both targeted observations and multispectral mapping. The summary products used in this paper are described by Murchie *et al.* [2009a]. CRISM data were analyzed in conjunction with HiRISE and CTX images that were processed to the standard levels delivered to the Planetary Data System [McEwen *et al.*, 2007; Malin *et al.*, 2007]. The CRISM and CTX data were mosaicked, and the component images are listed in Table 1.

[16] To assess the possible role of evaporite deposition in the formation of the ILDs, we constructed high-resolution ($0.25^\circ \times 0.25^\circ$) hydrological models of the Tharsis region using the approach of Andrews-Hanna *et al.* [2007]. The initial topography of Valles Marineris was defined using current MOLA elevations, modified by removing the ILDs and closing the outflow channels. However, no attempt was made to shrink the chasmata to their smaller sizes at the time of the layered deposits' emplacement. Also, crustal permeability was assumed to be uniform laterally, disregarding the possible enhanced permeability along fracture zones. We conservatively assumed a groundwater salinity comparable to seawater and incorporation of 60% by volume of clastics into precipitates [McLennan *et al.*, 2005]. More saline groundwater or more incorporation of clastics would result in more rapid accumulation of surface deposits. The model was run over 400 Ma, and the topography was modified continually as material accumulated over areas of groundwater discharge.

4. Results

4.1. Spectral Variations in the Layered Deposits

[17] Figure 1a shows the location of the study area in western Candor Chasma. Figures 2a and 2b are mosaics of

Table 1. List of CRISM and CTX Images Used to Assemble the Mosaics

CRISM Targeted Observations ^a	CRISM Multispectral Mapping Strips ^a	CTX Images ^b
FRT000039F3_07	MSP00003052_05	P02_001707_1744_XN_05S076W_061207
FRT0000400F_07	MSP0000317D_05	P02_001773_1745_XN_05S076W_061212
FRT00004694_07	MSP000032D3_05	P03_002063_1733_XI_06S075W_070104
FRT00005350_07	MSP000034A9_05	P06_003197_1736_XI_06S075W_070402
FRT00005521_07	MSP000034A9_07	P07_003830_1731_XI_06S075W_070521
FRT0000593E_07	MSP000035C0_07	P16_007232_1743_XN_05S076W_080210
FRT00005D17_07	MSP00003D1D_07	
FRT00006470_07	MSP00003D1E_01	
FRT000082C5_07	MSP0000416B_05	
FRT000098BB_07	MSP000042B7_07	
FRT00009A20_07	MSP00004A45_07	
FRT00009CB6_07	MSP00005B30_03	
FRT0000A938_07	MSP0000691F_05	
FRT0000B0F2_07	MSP00006FB4_07	
FRT0000B389_07		
HRL00002831_07		
HRL000033B7_07		
HRL00003E78_07		
HRL00008443_07		
HRL0000AB7A_07		

^aIn the CRISM file names, the first three characters designate the type of observation (full or half spatial resolution targeted observation, or multispectral mapping strip). The next eight characters are a unique hexadecimal identifier for each observation. The observations are typically multiimage, so the last two characters designate the component image from the observation.

^bOnly the CTX images shown in the figures are listed.

multispectral and targeted observations covering the study area, showing summary products indicative of major mineral phases to highlight characteristics of the ILDs and their differences from the chasma wall rock. Representative spectra of type locations of major spectral units identified are shown in Figure 3a. At the scale of kilometers, CRISM corroborates earlier observations from OMEGA data such as that the ILDs are distinct from the chasma wall rock, and the spatial distribution of major mineral phases [Mangold *et al.*, 2008]. However, the twentyfold increase in spatial resolution reveals new information on these phases' stratigraphy and distribution that leads to new geologic interpretations of how the materials containing these phases were emplaced.

[18] The most basic result is that, to the limit of CRISM's spatial resolution, the ILDs are distinct from wall rock. A 1- μm absorption due to mafic minerals (blue image plane in Figures 2a and 2b) occurs prevalently on the chasma walls and floor, but only locally on the ILDs in dark patches ranging from kilometers to only tens of meters in scale. A broad, shallow 2- μm absorption (black and dark green spectra in Figure 3a) in addition to the 1- μm feature indicates that pyroxene is the spectrally dominant mafic mineral in all of these areas (Figure 3b), consistent with basaltic lithologies typical of the southern plateau plains [Mustard *et al.*, 2005]. In contrast to the wall rock, the ILDs are dominated by medium- to high-albedo materials that exhibit a pervasive 0.53- μm band indicative of nanophase ferric oxide (red in Figures 2a and 2b, orange spectrum in Figure 3a). At wavelengths <1.4 μm , most light-toned parts of the ILDs are indistinct from dust on the surrounding plateau, and only dark, sandy materials and regions exhibiting absorptions due to crystalline ferric minerals are conspicuous.

[19] Spectra of the ILDs also exhibit absorptions indicative of hydrated sulfates and crystalline ferric minerals, which are absent from chasma wall rocks to the limit of

CRISM's spatial resolution. Ferric minerals are evidenced by absorptions near 0.53 and 0.9 μm [Sherman *et al.*, 1982; Morris *et al.*, 1985]. Monohydrated sulfates have characteristic absorptions near 2.1 and 2.4 μm ; in polyhydrated sulfates (with multiple bound water molecules), the shorter absorption occurs near 1.9 μm , and the 2.4- μm absorption becomes so strong that it transforms into a falloff in brightness past 2.3 μm (Figure 3b) [Hunt and Salisbury, 1971a; Rossman, 1976; Clark *et al.*, 1990; Cloutis *et al.*, 2006]. Hydrated sulfates are characteristic of the ILDs and their absorptions are recognized in most parts of the ILDs in Ceti Mensa and on the slopes of Candor Mensa. Figure 2b shows sulfates in green, as strength of the inflection in the spectrum is due to a 2.4- μm absorption. The sulfate signature is resolvable as numerous patches ranging from kilometers-scale, medium- and high-albedo outcrops seen in OMEGA data, to previously unresolved dark patches only tens to hundreds of meters in scale.

[20] In contrast to the spatially widespread spectral signature due to sulfates, enhanced absorptions due to crystalline ferric minerals are more localized. Figure 2a shows crystalline ferric minerals in green, as the strength of a 0.9- μm absorption. This absorption is absent from nanophase ferric oxides, but present in more crystalline, red- to gray-colored ferric oxides and many Fe sulfates with crystal ordering at scales of microns or greater. There are two types of exposures in which there is an enhanced 0.9- μm absorption: First, where there is also a 0.53- μm absorption due to nanophase oxides and invariably also a strong signature of hydrated sulfate (yellow in Figure 2a, red spectrum in Figure 3a). These exposures occur in medium- to high-albedo layers on the slopes of both plateaus. The second type of exposure has a weak 0.53- μm band, a grayer color at visible wavelengths, and a strong rise in reflectance into the infrared (green in Figure 2a, thick brown spectrum in Figure 3a). These exposures do not correspond with hydrated sulfates, and occur at the base of the plateaus' flanks

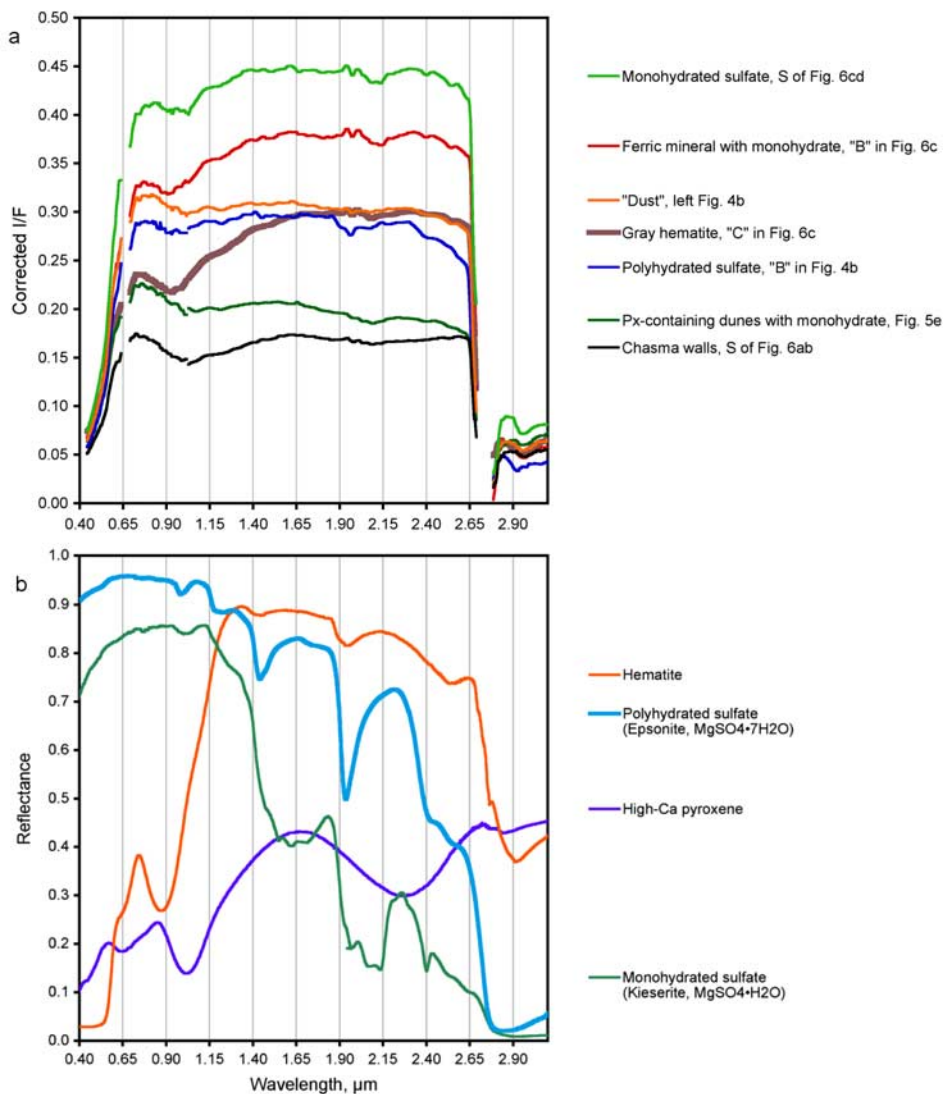


Figure 3. (a) Type spectra of materials discussed in the text, covering wavelengths 0.44–3.1 μm . Each spectrum covers a nearly square area of between 5×5 and 11×11 pixels, between 90 and 200 m on a side. The data have been calibrated to apparent I/F, divided by the cosine of the incidence angle, and divided by an atmospheric transmission spectrum scaled to strength of the 2.0- μm CO_2 absorption. Breaks in the spectra are wavelengths where data calibration is degraded. (b) Laboratory spectra of pure mineral analogs for material observed in western Candor Chasma.

or on the lowermost slopes. The largest occurrence, west of Candor Mensa, corresponds to TES detection of gray hematite [Mangold *et al.*, 2008]. However, this region's reflectance spectrum is not a close match to hematite (compared with the orange spectrum in Figure 3b): the 0.9- μm band in CRISM data is centered near 0.94 μm in contrast to the 0.85- to 0.89- μm band center present in hematite, and the 0.53- μm band is weaker than expected. This result suggests that other ferric phases may occur with the gray hematite, but no single phase can be conclusively identified owing to a lack of additional, diagnostic spectral features. Additional kilometers-scale, previously unrecognized exposures of crystalline ferric minerals occur at the base of the northeast and south flanks of Ceti Mensa. Smaller occurrences tens to hundreds of meters in scale

also occur, typically in lower-albedo patches interpreted as talus at the base of slopes, and in low-albedo dunes.

4.2. Stratigraphic Relations Within the Layered Deposits

[21] Five new findings from MRO data provide information that we used to develop the layered deposits' stratigraphy and to formulate and test a model for their origin. First, polyhydrated and monohydrated sulfates occur in discrete, sometimes intercalated layers, with polyhydrated sulfates higher in the stratigraphic section. The type example (Figure 4a) is on the northwestern flank of Ceti Mensa, where medium-albedo, flat-topped, erosion-resistant units A and B form steep-sided benches containing polyhydrated sulfate (blue spectrum in Figure 3a). The two units outcrop at elevations of +2450 m and +2200 m, respectively, and are

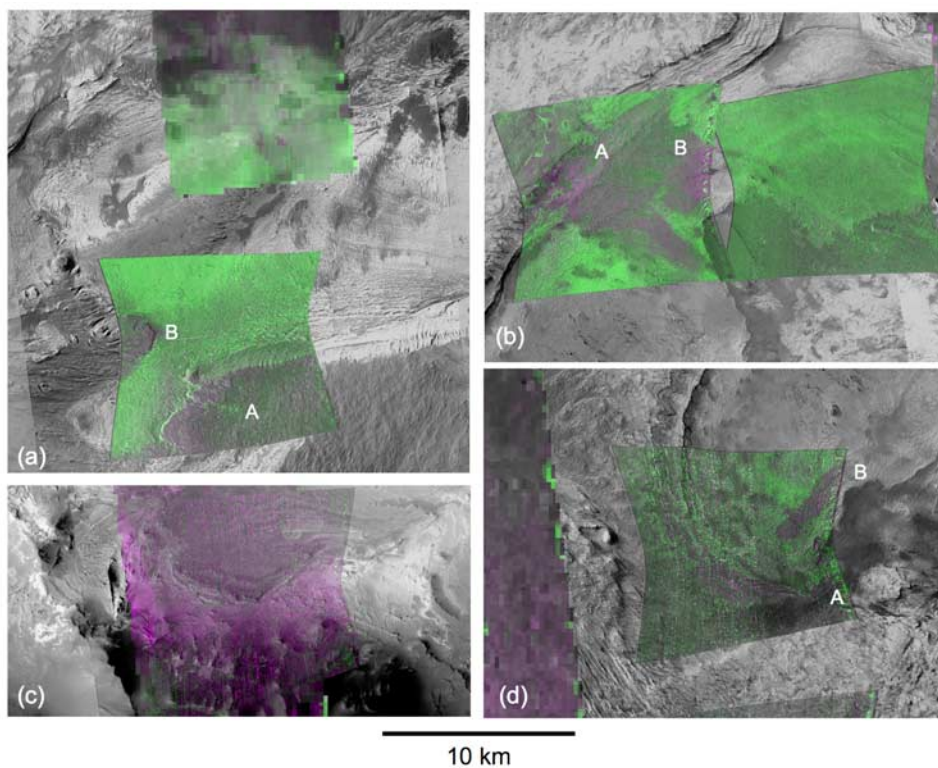


Figure 4. Summary product composites showing absorption strengths due to hydrated sulfates at the locations indicated in Figure 2. In each case (a–d), red and blue image planes from Figure 2 are depth of the 1.9- μm absorption due to polyhydrated sulfates (SINDEX), showing occurrences of polyhydrated sulfates in a magenta color, and the green image plane is depth of the 2.1- μm absorption due to monohydrated sulfates (SINDEX). All three image planes have a dynamic range of 0.04 and have been overlain on map-projected CTX images for context.

embedded within higher-albedo, monohydrated sulfate-containing materials (bright green spectrum in Figure 3a) that are more erodible and form slopes. Figures 4b and 4d show other high-resolution views of steep, eroded slopes at the same elevation range on the east flank Ceti Mensa. In both cases, upper and lower polyhydrated sulfate-rich units are visible (also marked A and B). Unit A is consistently cliff forming, whereas unit B is cliff forming in some locations and slope forming in others. The elevations of the A and B units are consistent to within ~ 400 m over 70 km distance. We interpret these outcrops to represent a pair of continuous, subhorizontal marker beds distinguished by their sulfate mineralogy. Sulfates higher in the section (e.g., to the left in Figure 3d) are commonly polyhydrated. Sulfates lower in the section but still within the mapped distribution of unit Hvl (Figure 1a) (e.g., to the right in Figure 4b and in Figure 5) have a consistently monohydrated signature.

[22] Second, hydrated sulfates occur within the valley floor material (unit Avf of Figure 1a) as well as in the ILDs. The valley floor material is thought to be stratigraphically younger than the ILDs themselves, as it infills low areas between the eroded plateaus [Scott and Tanaka, 1986; Witbeck et al., 1991]. In general, the valley floor material is dominated by a basaltic spectral signature exhibiting absorptions due to high-Ca pyroxene, and in CTX and HiRISE images the surface is commonly reworked into dunes or ripples. However, several small closed depressions provide erosional windows into deeper parts of the unit.

One of the higher-elevation examples, just below the 0 km elevation contour, is located off the south flank of Ceti Mensa (Figure 4c). In this and the other exposures of hydrated sulfates in valley floor material, polyhydrated sulfate is the dominant hydrated sulfate phase and typically it occurs with small exposures of crystalline ferric minerals. Other notable exposures lie off the northeast flank of Ceti Mensa at -2 km elevation, and south of Candor Mensa at -3 km elevation.

[23] The third finding is that erosional debris on Ceti and Candor Mensae has a sulfate signature dominated by monohydrated phases. Depending on the layer from which the debris originates, it also has the spectral signature of either crystalline ferric minerals or pyroxene. Figures 5a and 5b show an escarpment on the northeast flank of Ceti Mensa. Dark, pyroxene-containing streamers (bluish, at location A in Figure 5a) originate at the top of an escarpment and point downslope, and consist of loose material reformed by wind into ripples. Figure 5b shows that this streamer, as well as other material exposed along the same slope, also has a signature of monohydrated sulfate (green in Figure 5b). Above this steep slope, at location B in Figure 5a, dark, pyroxene- and monohydrated sulfate-bearing material also occurs at topographic steps in the layered exposure. Such dark materials on topographic steps are common on Ceti Mensa. Figures 5c and 5d show a large example on the plateau's eastern flank, using the same color scheme. The pyroxene and monohydrate signatures are even

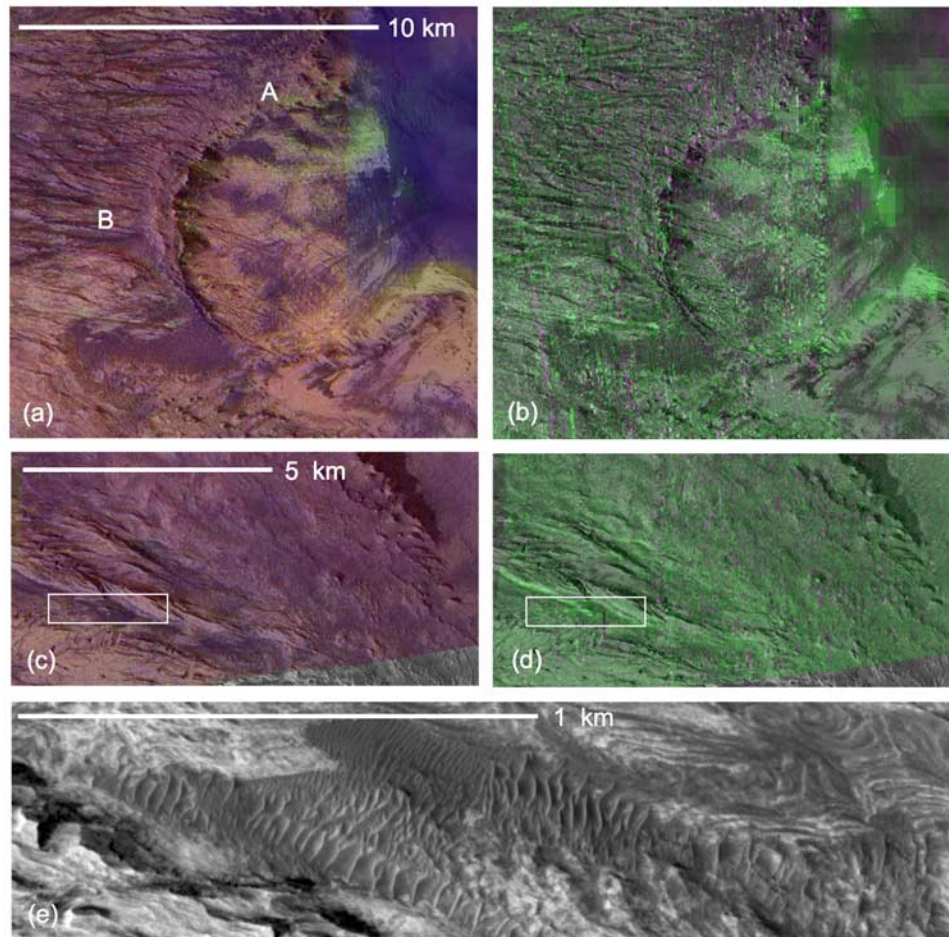


Figure 5. Examples of erosional debris occurring as ripples and streamers on slopes at the locations indicated in Figure 2. (a and c) Summary product composites showing the 0.53- μm , 0.9- μm , and 1- μm absorptions due to nanophase ferric oxide, crystalline ferric oxide, and pyroxene (BD5300, BD900, BDI1000VIS) in the red, green, and blue image planes, respectively, and were constructed identically to Figures 2a. All three image planes have been overlain on CTX images. (b and d) Depths of absorptions due to hydrated sulfates in the same area, using the same formulation as in Figure 4. (e) A portion of HiRISE image PSP_003830_1740_RED covering the white box in Figures 5c and 5d.

more pronounced (dark green spectrum in Figure 3a). Higher-resolution imaging by HiRISE (Figure 5e) shows that this and many other dark patches have been reworked by wind into ripples, and must at one time have been and may still be loose sand. The only examples of predominantly polyhydrated sulfate we see in dunes or ripples are adjacent to the polyhydrated sulfate-bearing units in Figures 4a and 4d, consistent with erosional debris from the layers. The presence of hydrated sulfates in these sands also shows that they are not simply erosional debris from the plateau plains draped over the ILDs, as suggested by *Mangold et al.* [2008], because the plateau plains lack the hydrated sulfate. Rather, the sands appear to originate from the ILDs themselves.

[24] A fourth finding is that dark monohydrated sulfate- and pyroxene-containing sand emanates from discrete strata within a section whose spectral signature of iron mineralogy is otherwise dominated by nanophase ferric oxide. Figure 6a shows a CRISM image of sulfate composition on the south flank of Ceti Mensa, overlain on a HiRISE image. Material with a weak polyhydrated sulfate signature forms erosion-resistant caprock, whereas darker monohydrated sulfate-

and pyroxene-bearing material forms the underlying slope, similar to other occurrences in topographic swales. The zoomed view in Figure 6b shows that sandy, monohydrated sulfate- and pyroxene-bearing material is eroding out of a friable layer. Similar dark friable layers are observed elsewhere in HiRISE images and have been interpreted as buried beds of basaltic sand [*Herkenhoff et al.*, 2007].

[25] The fifth finding is that crystalline ferric minerals have accumulated in debris aprons, fans, and eolian deposits in a manner suggesting that it originates in sulfate-containing beds in the layered deposits. Figure 6c shows the northwestern flank of Candor Mensa, where OMEGA and TES data suggested that gray hematite may be eroding out of a slope and accumulating at its base [*Mangold et al.*, 2008]. CRISM data strongly support this interpretation. Layers with a yellowish color (e.g., at location A) have a high albedo and a 0.53- μm absorption consistent with a dust-like composition, as well as a 0.9- μm band indicating one or more crystalline ferric minerals. Figure 7 shows a spectrum of this material, ratioed to nearby, more dust-like soils, and compared with a laboratory spectrum of hematite.

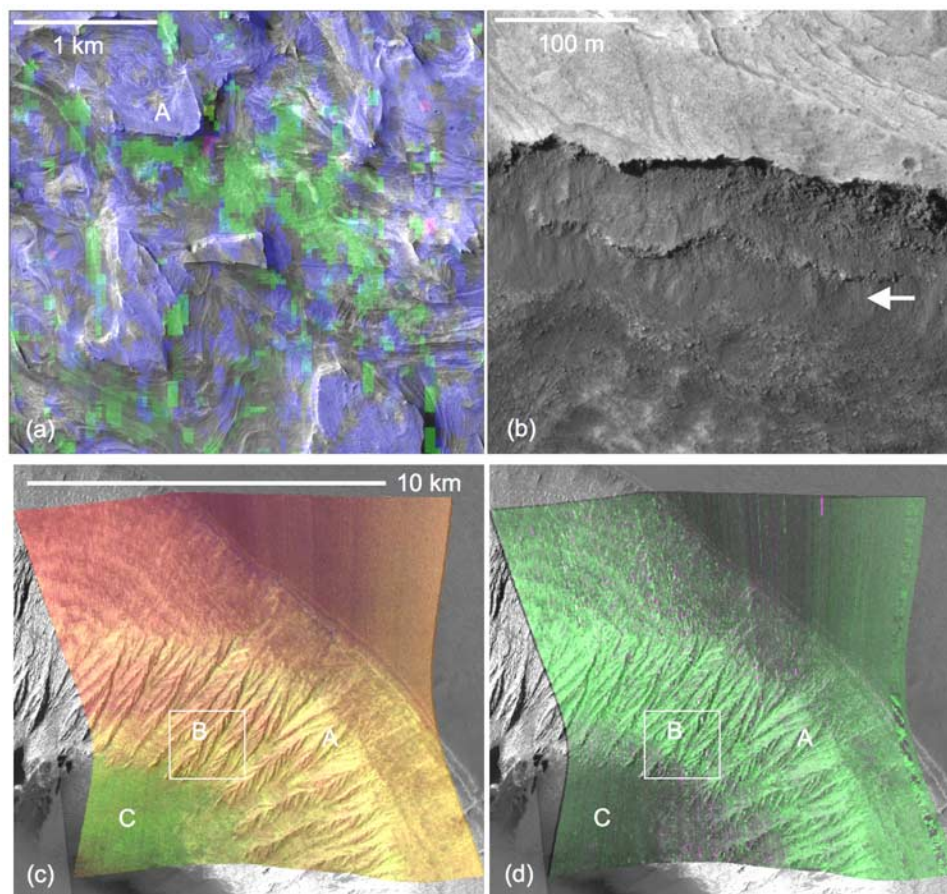


Figure 6. Examples of erosional debris traceable to specific strata or groups of strata in the layered deposits at the locations indicated in Figure 2. (a) An overlay of strengths of the 1.9- μm and 2.1- μm absorptions due to hydrated sulfate (BD1900, BD2100) in the blue and green image planes, respectively, on HiRISE image PSP_001641_1735. (b) Zoomed view of the scarp below location A in Figure 6a, showing correlation of stronger monohydrate absorptions with dark material that appears to be emanating from a friable layer beneath the lighter-toned, polyhydrate-containing ledge (arrow). (c) A summary product composite showing the 0.53- μm , 0.9- μm , and 1- μm absorptions due to nanophase ferric oxide, crystalline ferric oxide, and pyroxene (BD5300, BD900, BDI1000VIS) in the red, green, and blue image planes, respectively, and was constructed identically to Figures 5a and 5c. The white box shows the location of the HiRISE image in Figure 7. (d) Depths of absorptions due to hydrated sulfates in the same area, constructed identically to similar images in Figures 4 and 5. The locations of the box and lettering are the same as in Figure 6c.

Compared with dust, the crystalline ferric mineral exhibits stronger absorptions near 0.55 and 0.89 μm , a stronger shoulder at 0.6 μm , and a stronger reflectance peak at 0.75 μm , all of which are characteristic of hematite. The layers containing the enhanced signature of crystalline hematite are also monohydrated sulfate bearing (green in Figure 6d, red spectrum in Figure 3a). The hematite signature becomes stronger in chutes such as at location B in Figure 6a. The strongest signature is at the base of the slope at location C in Figure 6c, on a low, fan-like apron extending from the base of the chute. The surface of the apron is darker, grayer at visible wavelengths, has a weaker 0.53- μm band, the strongest observed 0.9- μm band, and sulfate absorptions are nearly absent (thick brown spectrum in Figure 3a).

[26] Figure 8a shows a HiRISE image of the chute at location B in Figure 6c and the surrounding chutes. The chutes are filled with braided deposits that empty into the

apron. Figure 8b is a higher-resolution view of one of the chutes showing that the braided pattern is characteristic of the floor of the chute and distinct from the surrounding ridges of eroded ILD material. The braids are discontinuously mantled by dark sand, which form a nearly continuous mantle on the lower part of the apron. These patterns are consistent with alluvial transport of coarse-grained, gray hematite originally dispersed within the ILD in a matrix, following the cessation of ILD emplacement and erosion to form the plateau. Fluid flow in such an alluvial environment could have removed the fines, concentrating the gray hematite in the apron at the base of the slope, where it has been further concentrated by eolian sorting. In addition subsequent mass wasting may have contributed to the cover of hematite-containing sand. The enhanced red hematite signature in the source beds and in the chutes is consistent with a fine-grained component accompanying the gray

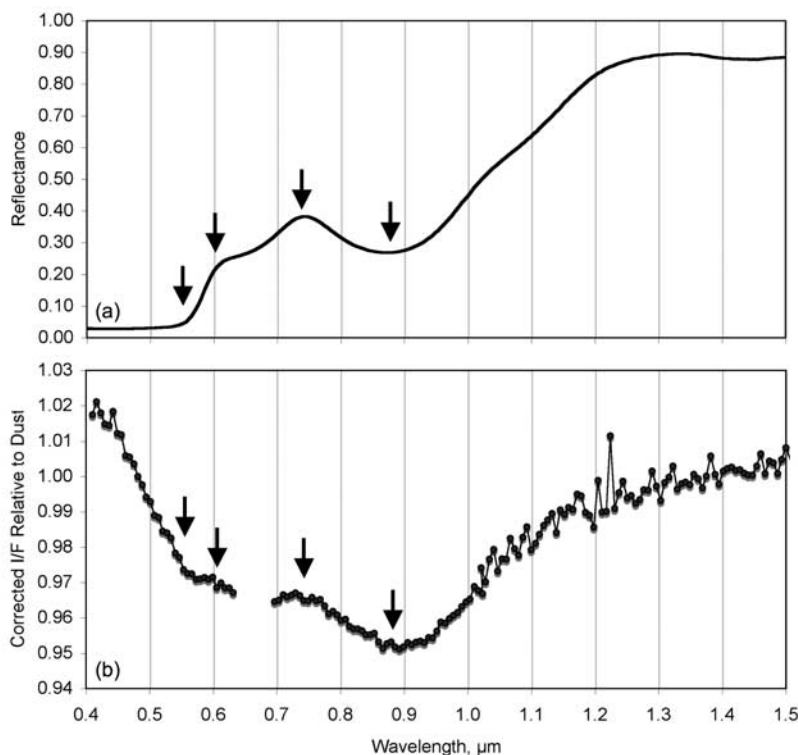


Figure 7. Laboratory spectrum of (a) finely crystalline hematite compared to the spectrum of (b) material in the chute at location A in Figure 6a, ratioed to nearby dust. The arrows denote absorptions at 0.55 and 0.89 μm , a shoulder in the spectrum at 0.6 μm , and a reflectance peak near 0.75 μm in the laboratory hematite that have counterparts in the ratio spectrum which indicate hematite to be present.

hematite or abraded from it during transport. As described in section 5.2, the source of the water could have been groundwater discharge, or possibly sediment dewatering.

4.3. Hydrologic Modeling

[27] The hydrologic model of the Valles Marineris region was run for 400 Ma beginning in the late Noachian period and extending into the middle Hesperian period. Areas of groundwater discharge initially include Valles Marineris, Echus Chasma, Solis Planum, and Chryse at the mouth of Kasei Vallis. As the system evolves, discharge outside of the chasmata diminishes owing to a drawdown cone formed by discharge into the chasmata, and extending ~ 300 km beyond the walls; however, groundwater flux across the Valles Marineris canyon floor remains steady at a rate of ~ 0.6 mm/a. The model predicts thin sediment accumulations in several locations outside the chasmata, and accumulation of a thick sequence of evaporite-cemented sediments within Valles Marineris (colored areas in Figure 1b). Discharge is maintained even as the chasmata infill with sediment, because hydraulic head is maintained. However, as drawdown continues, discharge becomes increasingly focused at the lowest elevations of the chasmata.

[28] A maximum thickness of ~ 5 km of evaporite-cemented eolian sediment is predicted to accumulate in western Candor Chasma after ~ 400 Ma. The modeled deposit thicknesses are strongly sensitive to the assumed precipitation rate and aquifer permeability, to high-permeability zones between individual lava flow units within Tharsis [Hanna and Phillips, 2005], to channeling

of fluids by the Valles Marineris canyon faults which would accelerate accumulation, and to the original shapes and extents of the chasmata. Thus the predicted thicknesses are only approximate.

[29] The predicted extent of the deposits encloses not only the ILDs in western Candor Chasma, but also other major occurrences in Tithonium, Ophir, eastern Candor, Melas, Eos, and Ganges Chasmata (outlined in yellow in Figure 1b). With the exception of Eos Chasma, the model also accurately predicts the thickest accumulations where the ILDs are observed today. Another interesting result is that the predicted area of sediment accumulation within the chasmata is closely matched by the combination of areas covered by the Hesperian-aged ILDs (unit Hvl in Figure 1a) and the Amazonian-aged valley fill materials (unit Avf). As discussed above, hydrated sulfates are part of the series of deposits forming unit Avf, except covered with sand and other materials in most locations. Given that groundwater discharge is predicted to have been longest lasting in the lowest parts of the chasmata, this raises the possibility that as chasma walls receded and the initial ILD deposits were eroded, accumulation of sulfate-bearing sediment could have continued on the chasma floor. In addition, alluvial transport of fines from the eroding slopes of ILD plateaus could have contributed to lower beds of the valley fill material.

5. Discussion

5.1. Geologic Sequence of Events

[30] The prevalence of monohydrated sulfates both in intact outcrops and in erosional debris is extremely signif-

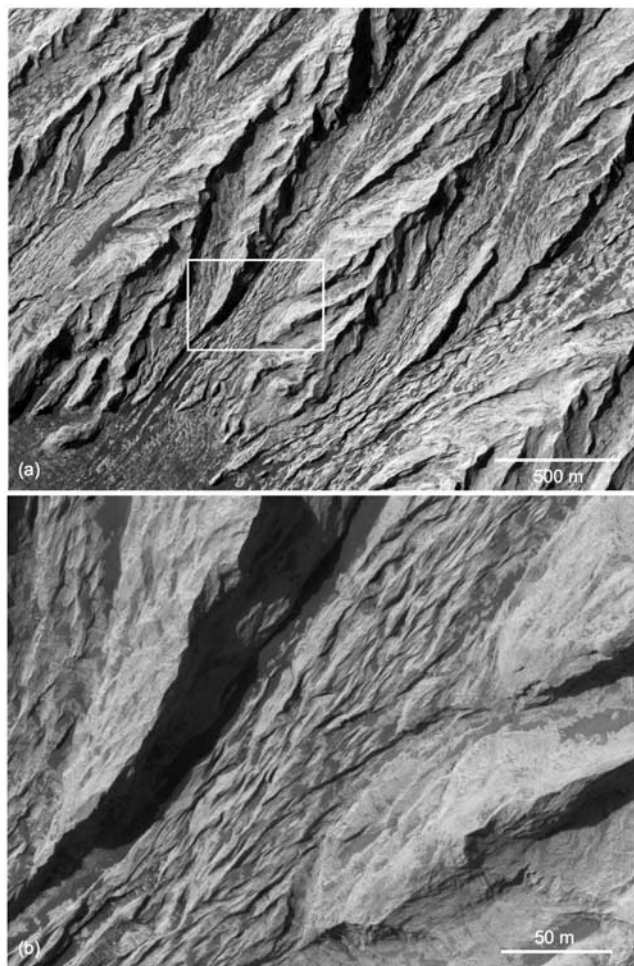


Figure 8. Part of HiRISE image PSP_007166_1740_RED. (a) Braided channels filling the chutes upslope from the concentration of gray hematite at the base of Candor Mensa. (b) A higher-resolution view of braids in one of the chutes showing that distinct morphology compared to the ridges between the chutes.

icant, because laboratory studies suggest that monohydrate at Mars' surface is unstable and should be altering to polyhydrate [e.g., *Vaniman et al.*, 2004]. Instead, sulfate phase changes must be slow compared to the time scale for formation of the optical surface of dunes and slope features, which is likely measured in thousands of years or longer. Possible reasons for the persistence of monohydrate include slow kinetics of phase changes at cold Martian surface temperatures [*Chipera and Vaniman*, 2007], the fact that most of the diurnal temperature cycle currently lies within the monohydrate stability field [*Roach et al.*, 2009], or intermixture of phases that inhibit the transition to more hydrated states [*Freeman et al.*, 2007]. The implication for interpreting spectral data is that variations in sulfate spectral signatures observed at the surface can represent subsurface compositions, and reveal sulfate stratigraphy. The observation from OMEGA data that polyhydrated sulfates tend to occur on flatter slopes than do monohydrated sulfates can be explained by the geologic setting of the polyhydrates, rather than by hydration of monohydrated sulfate-containing debris that has accumulated in flat areas: the polyhydrates

outcrop predominantly in the upper, flatter parts of Ceti Mensa, they commonly form gently sloping caprocks and benches, and they occur as small outcrops where the gently sloped valley floor material has been exhumed.

[31] Monohydrated and polyhydrated sulfates may occur in different beds of the ILDs because monohydrated sulfates precipitated under the most saline conditions and polyhydrated sulfates under less saline conditions, or because polyhydrated sulfates were diagenetically altered into monohydrated sulfates. Polyhydrated sulfates overlie monohydrated sulfates in most of the chasmata, suggesting a phase change at depth due to geothermal heating. *Garrett* [1995] showed that epsomite would convert to kieserite between 25°C and 40°C. Assuming a geothermal gradient of about 10 K/km [*Hoffman*, 2001], that is equivalent to burial to a few km, attained in the lower parts of western Candor Chasma and other thick ILDs. However, sulfate types have sharp, traceable contacts, and commonly are interbedded in multiple layers. These latter observations are inconsistent with a gradational change in phase with depth due to thermal alteration, but could be consistent with diagenesis where structural control, perhaps along bedding planes, played a major role in flow of diagenetic fluids [e.g., *Eichhubl et al.*, 2004]. Alternatively, these observations could be consistent with different sulfate phases having been deposited originally. In the latter case, elevated temperatures at depth may have prevented postdepositional alteration of monohydrate to polyhydrate if the source fluids of the polyhydrate percolated through it.

[32] Key results from CRISM measurements can be used to constrain the stratigraphy of the ILDs, which is illustrated as a highly schematic geologic cross section in Figure 9. Sulfates in the lower and middle parts of the section are dominated by monohydrate. Most sulfate-bearing layers have a high albedo and a 0.53- μm absorption consist with nanophase ferric oxide, which dominates dust. Rarely, sulfate-bearing layers shed dune-forming sand with pyroxene absorptions like those in the chasma walls and surrounding plateau. Polyhydrated sulfates occur in throughgoing layers, typically high in the section and overlain by monohydrate. Finally, many of the sulfate-bearing strata also contain dispersed crystalline ferric minerals, including a coarse, gray fraction containing gray hematite that gets concentrated by slope processes. These characteristics bear many resemblances to layered deposits in Meridiani Planum: the deposits in Meridiani are also dominated spectrally by nanophase ferric oxide, are mixed and intercalated with pyroxene-containing sand, contain dispersed crystalline ferric minerals, host concretions of gray hematite that are concentrated as lag deposits by erosion, and contain discrete strata exhibiting spectral signatures of monohydrated and polyhydrated sulfates [*Arvidson et al.*, 2006; *Griffes et al.*, 2007; *Wiseman et al.*, 2007].

[33] The history of emplacement of morphologic units in western Candor Chasma reconstructed from HiRISE terrain models [*Okubo et al.*, 2008] complements CRISM measurements of the compositional layering of the ILDs. Okubo et al.'s derived history includes draping of fine-grained sediment over the chasma interior subsequent to downdropping of the floor, contemporaneous or postdepositional folding and faulting of the sediments, and erosion to form early

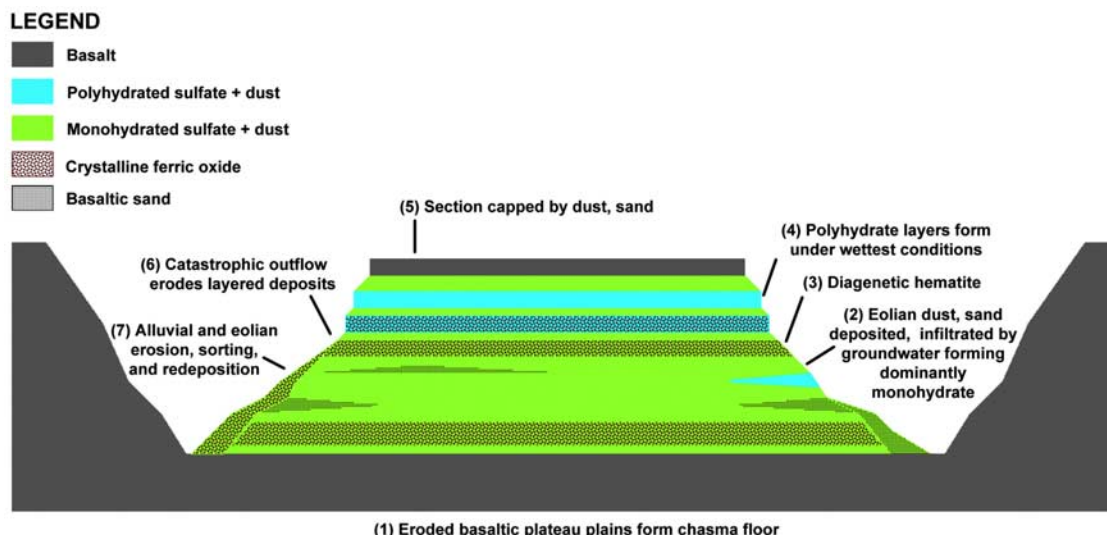


Figure 9. Schematic cross section of layered deposits in western Candor Chasma. The interpreted sequence of events in forming the deposits is numbered.

versions of the present plateaus. Evidence for the presence of fluids within the stack of layered sediments includes narrow reddened, possibly mineralized zones along faults [Okubo and McEwen, 2007], and folding of layered deposits on the southwestern floor of the chasma [Okubo *et al.*, 2008]. The ILDs' streamlined shapes and their location in a source region for outflow channels have long been interpreted as evidence for a role of catastrophic flow of liquid late in or after the deposits' emplacement [Lucchitta *et al.*, 1992].

5.2. Relationship to Groundwater Discharge

[34] On the basis of these new results, we propose that the interior layered deposits in western Candor Chasma originated in a manner analogous to the layered deposits in Meridiani Planum. Sulfates deposited in regions of groundwater discharge trapped, cemented, and lithified layers of eolian dust and sand, and diagenetic alteration of the sediments formed the coarse-grained hematite.

[35] A sequence of events whereby groundwater discharge could have contributed to layered deposit formation is outlined in Figure 9. Interbedded eolian sand and dust accumulated on the chasma floor where the groundwater intersected the surface, evaporating and created hypersaline conditions in which sulfates precipitated, trapping and lithifying the sediments. Crystalline hematite formed during diagenesis. Later and higher in the section, polyhydrated sulfates formed. The compositional difference between sulfate phases, with monohydrates stratigraphically low in the section and polyhydrates stratigraphically high in the section, could result from several possible origins: long-term changes in climate or discharge rate that led to less saline conditions later during formation of the ILDs, or burial of polyhydrated sulfates and diagenesis to form monohydrate, with polyhydrate preserved preferentially in zones of high groundwater flow. Ultimately, a combination of gradual eolian erosion and catastrophic discharge of groundwater or water-laden sediment eroded the plateaus to nearly their present form. Small amounts of sulfate-cemented sediment continued to accumulate in the valley

floor material, and dewatering of sediment from springs on the exposed flanks of the plateaus and/or continued groundwater discharge formed alluvial fans with surfaces enriched in coarse-grained hematite. Once groundwater discharge ceased, eolian erosion and redeposition formed the rippled sand deposits.

[36] This model can explain the concentration of sulfates in the layered deposits not predicted by subaerial volcanism [Lucchitta *et al.*, 1992] or eolian or pyroclastic sedimentation [Peterson, 1981], or if the layered deposits are remnants of the chasma wall [Edgett and Malin, 2003]. It also accounts for changes in sulfate composition that would require ad hoc explanation in an ice-covered lacustrine environment [Nedell *et al.*, 1987]. If this model is substantiated by future tests and continued analysis of MRO data, it could link the widely separated layered deposits in Meridiani Planum and Valles Marineris to the common process of accumulation of eolian sediments where they are trapped by evaporites precipitated by groundwater discharge.

[37] The major difference between the ILDs and layered deposits in Meridiani Planum that is apparent from orbit, the folding and fracturing of the deposits in Valles Marineris, could be largely a result of the ILDs' geologic setting in the Valles Marineris chasmata. In Planum Meridiani the layered deposits accumulated on rolling, cratered plains to a thickness of hundreds of meters [Arvidson *et al.*, 2003]. In contrast, in Valles Marineris they accumulated to kilometers in thickness within steep-sided chasmata. In the distal regions of the ILDs in western Candor Chasma, this setting resulted in bedding that dips inward toward the center of the chasma, driving gravity-driven deformation including folding and faulting that is largely lacking in Meridiani Planum [Okubo *et al.*, 2008].

6. Summary and Conclusions

[38] The interior layered deposits of the Valles Marineris region were investigated using new results from the CRISM, HiRISE, and CTX instruments on MRO, focusing on western Candor Chasma where the layered deposits are

particularly well exposed owing to a paucity of dust and the thickness of the deposits. The spectrally dominant phases in most of these ILDs are monohydrated sulfates and nano-phase ferric oxides/oxyhydroxides. Basaltic sand with a spectral signature of pyroxene is also observed, and appears to be interbedded with the monohydrated sulfate-bearing layers. Many of the sulfate-rich layers also exhibit visible wavelength spectral features consistent with ferric minerals. A coarse-grained grayer component that is dispersed in the deposits has been concentrated locally by sorting and alluvial processes, and is attributed to coarse-grained hematite observed by TES. Some of ILDs at higher elevations contain polyhydrated sulfates implying chasma-scale changes in the abundance of liquid water or brine chemistry during formation of the layered deposits.

[39] High-resolution hydrological models were constructed in order to gain a better understanding of the layered deposits observed by CRISM. The model predicts thin sediment accumulations outside the chasmata, but accumulation of a thick sequence of evaporite-cemented sediments within Valles Marineris. A predicted thickness of ~5 km of sediments in western Candor Chasma closely matches the observed thickness of the ILDs, and the predicted spatial distribution of the accumulations matches the coverage of the combined ILDs and the sulfate-bearing valley floor materials between them.

[40] The Candor Chasma ILDs are consistent with lithification of eolian dust, sand, and ash by evaporites predicted to have formed within the chasma by evaporation of groundwater discharge. This would have created hypersaline conditions in which monohydrated sulfates precipitated. Contemporaneous diagenetic alteration is believed to have formed crystalline hematite. Polyhydrated sulfates would have formed at late during the ILDs' deposition when changes in climate or discharge rate lessened salinity.

[41] Coordinated analyses of the model results and CRISM observations provide a link between the layered deposits observed in Valles Marineris and those in Meridiani Planum. Both regions are characterized by sulfates and ferric oxides in layered deposits. The large-scale hydrologic modeling presented here and the similarity in sediments at both sites suggest that a common regional process was responsible for forming sulfate-bearing deposits both sites.

[42] **Acknowledgments.** The authors thank the CRISM, HiRISE, CTX, and MRO operations team for collecting the data that made the results in this paper possible. This work was supported by MRO funding through subcontract 852950 from the Jet Propulsion Laboratory.

References

- Adams, J. (1974), Visible and near-infrared diffuse reflectance spectra of pyroxenes as applied to remote sensing of solid objects in the solar system, *J. Geophys. Res.*, *79*, 4829–4836, doi:10.1029/JB079i032p04829.
- Andrews-Hanna, J., R. Phillips, and M. Zuber (2007), Meridiani Planum and the global hydrology of Mars, *Nature*, *446*, 163–168, doi:10.1038/nature05594.
- Arvidson, R. E., F. Seelos IV, K. Deal, W. Koeppen, N. Snider, J. Kieniewicz, B. Hynek, M. Mellon, and J. Garvin (2003), Mantled and exhumed terrains in Terra Meridiani, Mars, *J. Geophys. Res.*, *108*(E12), 8073, doi:10.1029/2002JE001982.
- Arvidson, R. E., F. Poulet, J.-P. Bibring, M. Wolff, A. Gendrin, R. V. Morris, J. J. Freeman, Y. Langevin, N. Mangold, and G. Bellucci (2005), Spectral reflectance and morphologic correlations in eastern Terra Meridiani, Mars, *Science*, *307*, 1591–1594, doi:10.1126/science.1109509.
- Arvidson, R. E., et al. (2006), Nature and origin of the hematite-bearing plains of Terra Meridiani based on analyses of orbital and Mars Exploration rover data sets, *J. Geophys. Res.*, *111*, E12S08, doi:10.1029/2006JE002728.
- Bibring, J.-P., et al. (2005), Mars surface diversity as revealed by the OMEGA/Mars Express observations, *Science*, *307*, 1576–1581, doi:10.1126/science.1108806.
- Bibring, J.-P., et al. (2006), Global mineralogical and aqueous Mars history derived from OMEGA/Mars Express data, *Science*, *312*, 400–404, doi:10.1126/science.1122659.
- Bibring, J.-P., et al. (2007), Coupled ferric oxides and sulfates on the Martian surface, *Science*, *317*, 1206–1210, doi:10.1126/science.1144174.
- Bishop, J., et al. (2007), Sulfates and mafic minerals in Juventae Chasma as seen by CRISM in coordination with OMEGA, HiRISE and context images, in *Seventh International Conference on Mars, July 9–13, 2007, Pasadena CA* [CD-ROM], *LPI Contrib.*, *1353*, Abstract 3350.
- Bishop, J., et al. (2009), Mineralogy of Juventae Chasma: Sulfates in the light-toned mounds, mafics in the sand, and opal in the plains, *J. Geophys. Res.*, doi:10.1029/2009JE003352, in press.
- Chipera, S. J., and D. T. Vaniman (2007), Experimental stability of magnesium sulfate hydrates that may be present on Mars, *Geochim. Cosmochim. Acta*, *71*, 241–250, doi:10.1016/j.gca.2006.07.044.
- Christensen, P. R., R. V. Morris, M. D. Lane, J. L. Bandfield, and M. C. Malin (2001), Global mapping of Martian hematite mineral deposits: Remnants of water-driven processes on early Mars, *J. Geophys. Res.*, *106*, 23,873–23,885, doi:10.1029/2000JE001415.
- Clark, R., T. King, M. Klejwa, G. Swayze, and N. Vergo (1990), High resolution gelation reflectance spectroscopy of minerals, *J. Geophys. Res.*, *95*, 12,653–12,680, doi:10.1029/JB095iB08p12653.
- Cloutis, E. A., and M. Gaffey (1991), Pyroxene spectroscopy revisited: Spectral-compositional correlations and relationship to geothermometry, *J. Geophys. Res.*, *96*, 22,809–22,826, doi:10.1029/91JE02512.
- Cloutis, E. A., et al. (2006), Detection and discrimination of sulfate minerals using reflectance spectroscopy, *Icarus*, *184*, 121–157, doi:10.1016/j.icarus.2006.04.003.
- Edgett, K., and M. Malin (2003), The layered upper crust of Mars: An update on MGS MOC observations after two Mars years in the mapping orbit, *Lunar Planet. Sci.*, *XXXIV*, Abstract 1124.
- Ehlmann, B., et al. (2008), Orbital identification of carbonate-bearing rocks on Mars, *Science*, *322*, 1828–1832, doi:10.1126/science.1164759.
- Eichhubl, P., W. Lansing Taylor, D. Pollard, and A. Aydin (2004), Paleofluid flow and deformation in the Aztec Sandstone at the Valley of Fire, Nevada—Evidence for the coupling of hydrogeologic, diagenetic, and tectonic processes, *Geol. Soc. Am. Bull.*, *116*, 1120–1136, doi:10.1130/B25446.1.
- Freeman, J. J., A. Wang, and B. L. Jolliff (2007), Pathways to form kieserite from epsomite at mid to low temperatures, with relevance to Mars, *Lunar Planet. Sci.*, *XXXVIII*, Abstract 1298.
- Garrett, D. E. (1995), *Potash: Deposits, Processing, Properties, and Uses*, 734 pp., Springer, New York.
- Gendrin, A., et al. (2005a), Sulfates in Martian layered terrains: The OMEGA/Mars Express view, *Science*, *307*, 1587–1591, doi:10.1126/science.1109087.
- Gendrin, A., et al. (2005b), Identification of predominant ferric signatures in association to the Martian sulfate deposits, *Lunar Planet. Sci.*, *XXXVI*, Abstract 1378.
- Glotch, T. D., and P. R. Christensen (2005), Geologic and mineralogic mapping of Aram Chaos: Evidence for a water-rich history, *J. Geophys. Res.*, *110*, E09006, doi:10.1029/2004JE002389.
- Griffes, J. L., R. E. Arvidson, F. Poulet, and A. Gendrin (2007), Geologic and spectral mapping of etched terrain deposits in northern Meridiani Planum, *J. Geophys. Res.*, *112*, E08S09, doi:10.1029/2006JE002811.
- Hanna, J., and R. Phillips (2005), Hydrological modeling of the Martian crust with an application to the pressurization of aquifers, *J. Geophys. Res.*, *110*, E01004, doi:10.1029/2005JE002546.
- Herkenhoff, K. E., S. Byrne, P. S. Russell, K. E. Fishbaugh, and A. S. McEwen (2007), Meter-scale morphology of the north polar region of Mars, *Science*, *317*, 1711–1715, doi:10.1126/science.1143544.
- Hoffman, N. (2001), Modern geothermal gradients on Mars and implications for subsurface liquids, paper presented at Conference on Geophysical Detection of Subsurface Water on Mars, Abstract 7044, Lunar Planet. Inst., Houston, Tex.
- Hunt, G., and J. Salisbury (1971a), Visible and infrared spectra of minerals and rocks. IV: Sulphides and sulphates, *Mod. Geol.*, *3*, 1–14.
- Hunt, G. R., and J. W. Salisbury (1971b), Visible and near infrared spectra of minerals and rocks. II: Carbonates, *Mod. Geol.*, *2*, 23–30.
- Klingelhöfer, G., et al. (2004), Jarosite and hematite at Meridiani Planum from Opportunity's Mössbauer Spectrometer, *Science*, *306*, 1740–1745, doi:10.1126/science.1104653.

- Komatsu, G., P. E. Geissler, R. G. Strom, and R. B. Singer (1993), Stratigraphy and erosional landforms of layered deposits in Valles Marineris, Mars, *J. Geophys. Res.*, *98*, 11,105–11,121, doi:10.1029/93JE00537.
- Lucchitta, B., et al. (1992), The canyon system on Mars, in *Mars*, edited by H. Kieffer et al., pp. 453–492, Univ. of Ariz. Press, Tucson.
- Lucchitta, B., N. K. Isbell, and A. Howington-Kraus (1994), Topography of Valles Marineris: Implications for erosional and structural history, *J. Geophys. Res.*, *99*, 3783–3798, doi:10.1029/93JE03095.
- Malin, M. C., et al. (2007), Context camera investigation on board the Mars Reconnaissance Orbiter, *J. Geophys. Res.*, *112*, E05S04, doi:10.1029/2006JE002808.
- Mangold, N., A. Gendrin, B. Gondet, S. LeMouelic, C. Quantin, V. Ansan, J.-P. Bibring, Y. Langevin, P. Masson, and G. Neukum (2008), Spectral and geological study of the sulfate-rich region of West Candor Chasma, Mars, *Icarus*, *194*, 519–543, doi:10.1016/j.icarus.2007.10.021.
- McEwen, A. S., et al. (2007), Mars Reconnaissance Orbiter's High Resolution Imaging Science Experiment (HiRISE), *J. Geophys. Res.*, *112*, E05S02, doi:10.1029/2005JE002605.
- McKay, C., and S. Nedell (1988), Are there carbonate deposits in the Valles Marineris, Mars?, *Icarus*, *73*, 142–148, doi:10.1016/0019-1035(88)90088-7.
- McLennan, S. M., et al. (2005), Provenance and diagenesis of the evaporite-bearing Burns formation, Meridiani Planum, Mars, *Earth Planet. Sci. Lett.*, *240*, 95–121, doi:10.1016/j.epsl.2005.09.041.
- Milliken, R., et al. (2008), Opaline silica in young deposits on Mars, *Geology*, *36*, 847–850, doi:10.1130/G24967A.1.
- Morris, R. V., H. V. Lauer Jr., C. A. Lawson, E. K. Gibson Jr., G. A. Nace, and C. Stewart (1985), Spectral and other physicochemical properties of submicron powders of hematite (α -Fe₂O₃), maghemite (γ -Fe₂O₃), magnetite (Fe₃O₄), goethite (α -FeOOH), and lepidocrocite (γ -FeOOH), *J. Geophys. Res.*, *90*, 3126–3144, doi:10.1029/JB090iB04p03126.
- Murchie, S., et al. (2007a), Compact Reconnaissance Imaging Spectrometer for Mars (CRISM) on Mars Reconnaissance Orbiter (MRO), *J. Geophys. Res.*, *112*, E05S03, doi:10.1029/2006JE002682.
- Murchie, S., et al. (2007b), CRISM mapping of layered deposits in western Candor Chasma, in *Seventh International Conference on Mars, July 9–13, 2007, Pasadena CA* [CD-ROM], *LPI Contrib.*, *1353*, Abstract 3238.
- Murchie, S. L., et al. (2009a), A synthesis of Martian aqueous mineralogy after one Mars year of observations from the Mars Reconnaissance Orbiter, *J. Geophys. Res.*, doi:10.1029/2009JE003342, in press.
- Murchie, S. L., et al. (2009b), The CRISM investigation and data set from the Mars Reconnaissance Orbiter's primary science phase, *J. Geophys. Res.*, doi:10.1029/2009JE003344, in press.
- Mustard, J. F., F. Poulet, A. Gendrin, J.-P. Bibring, Y. Langevin, B. Gondet, N. Mangold, G. Bellucci, and F. Altieri (2005), Olivine and pyroxene diversity in the crust of Mars, *Science*, *307*, 1594–1597, doi:10.1126/science.1109098.
- Mustard, J., et al. (2008), Hydrated silicate minerals on Mars observed by the CRISM instrument on MRO, *Nature*, *454*, 305–309, doi:10.1038/nature07097.
- Nedell, S., S. Squyres, and D. Andersen (1987), Origin and evolution of the layered deposits in the Valles Marineris, Mars, *Icarus*, *70*, 409–441, doi:10.1016/0019-1035(87)90086-8.
- Okubo, C. H., and A. S. McEwen (2007), Fracture-controlled paleo-fluid flow in Candor Chasma, Mars, *Science*, *315*, 983–985, doi:10.1126/science.1136855.
- Okubo, C. H., K. L. Lewis, A. S. McEwen, and R. L. Kirk (2008), Relative age of interior layered deposits in southwest Candor Chasma based on high-resolution structural mapping, *J. Geophys. Res.*, *113*, E12002, doi:10.1029/2008JE003181.
- Parente, M. (2008), A new approach to denoising CRISM images, *Lunar Planet. Sci.*, XXXIX, Abstract 2528.
- Pelkey, S. M., et al. (2007), CRISM multispectral summary products: Parameterizing mineral diversity on Mars from reflectance, *J. Geophys. Res.*, *112*, E08S14, doi:10.1029/2006JE002831.
- Peterson, C. (1981), A secondary origin for the central plateau of Hebes Chasma, *Proc. Lunar Planet. Sci. Conf.*, *12th*, 1459–1471.
- Poulet, F., J.-P. Bibring, J. F. Mustard, A. Gendrin, N. Mangold, Y. Langevin, R. E. Arvidson, B. Gondet, C. Gomez, and the OMEGA Team (2005), Phyllosilicates on Mars and implications for the early Mars history, *Nature*, *438*, 623–627, doi:10.1038/nature04274.
- Roach, L. H., J. F. Mustard, S. L. Murchie, J. L. Bishop, C. M. Weitz, A. T. Knudson, J.-P. Bibring, S. M. Pelkey, B. L. Ehlmann, and the CRISM Science team (2007), Magnesium and iron sulfate variety and distribution in east Candor and Capri Chasma, Valles Marineris, in *Seventh International Conference on Mars, July 9–13, 2007, Pasadena CA* [CD-ROM], *LPI Contrib.*, *1353*, Abstract 3223.
- Roach, L. H., J. F. Mustard, S. L. Murchie, J.-P. Bibring, R. E. Arvidson, J. L. Bishop, R. E. Milliken, F. Seelos, and the CRISM Science Team (2008), Constraints on the rate of sulfate phase changes in Valles Marineris interior layered deposits, *Lunar Planet. Sci.*, XXXIX, Abstract 1823.
- Roach, L. H., J. F. Mustard, S. L. Murchie, J.-P. Bibring, F. Forget, K. W. Lewis, O. Aharonson, M. Vincendon, and J. L. Bishop (2009), Testing evidence of recent hydration state change in sulfates on Mars, *J. Geophys. Res.*, *114*, E00D02, doi:10.1029/2008JE003245.
- Rossman, G. (1976), Spectroscopic and magnetic studies of ferric iron hydroxy sulfates: The series Fe(OH)SO₄ · nH₂O and jarosite, *Am. Mineral.*, *61*, 398–401.
- Scott, D., and K. Tanaka (1986), Geologic map of the western equatorial region of Mars, *U.S. Geol. Surv. Misc. Invest. Map*, *I-1802-A*.
- Sherman, D., R. Burns, and V. Burns (1982), Spectral characteristics of the iron oxides with application to the Martian bright region mineralogy, *J. Geophys. Res.*, *87*, 10,169–10,180, doi:10.1029/JB087iB12p10169.
- Solomon, S., et al. (2005), New perspectives on ancient Mars, *Science*, *307*, 1214–1220, doi:10.1126/science.1101812.
- Squyres, S. W., et al. (2006), Overview of the Opportunity Mars Exploration Rover mission to Meridiani Planum: Eagle Crater to Purgatory Ripples, *J. Geophys. Res.*, *111*, E12S12, doi:10.1029/2006JE002771.
- Sunshine, J., C. Pieters, and S. Pratt (1990), Deconvolution of mineral absorption bands: An improved approach, *J. Geophys. Res.*, *95*, 6955–6966, doi:10.1029/JB095iB05p06955.
- Tanaka, K. N., D. H. Scott, and R. Greeley (1992), Global stratigraphy, in *Mars*, edited by H. H. Kieffer et al., pp. 345–383, Univ. of Ariz. Press, Tucson.
- Vaniman, D. T., et al. (2004), Magnesium sulfate salts and the history of water on Mars, *Nature*, *431*, 663–665, doi:10.1038/nature02973.
- Wiseman, S. M., J. L. Griffes, R. E. Arvidson, S. Murchie, F. Poulet, A. T. Knudson, F. P. Seelos, N. Tosca, and the CRISM Science Team (2007), New analyses of MRO CRISM, HiRISE, and CTX data over layered sedimentary deposits in Meridiani, in *Seventh International Conference on Mars, July 9–13, 2007, Pasadena CA* [CD-ROM], *LPI Contrib.*, *1353*, Abstract 3111.
- Witbeck, N., K. Tanaka, and D. Scott (1991), Geologic map of the Valles Marineris region of Mars, *U.S. Geol. Surv. Misc. Invest. Map*, *I-2010*.

J. Andrews-Hanna, Department of Geophysics, Colorado School of Mines, Golden, CO 80401, USA.

R. Arvidson, K. Lichtenberg, and S. Wiseman, Department of Earth and Planetary Sciences, Washington University, St. Louis, MO 63130, USA.

J.-P. Bibring, Institut d'Astrophysique Spatiale, Batiment 120, Orsay F-91405, France.

J. Bishop, SETI Institute, 515 North Whisman Road, Mountain View, CA 94043, USA.

R. Milliken, NASA JPL, 4800 Oak Grove Drive, Pasadena, CA 91109, USA.

R. Morris, NASA JSC, 2101 NASA Parkway, Houston, TX 77058, USA.
S. Murchie and F. Seelos, Johns Hopkins University Applied Physics Laboratory, Laurel, MD 20723, USA. (scott.murchie@jhuapl.edu)

J. Mustard and L. Roach, Department of Geological Sciences, Brown University, Providence, RI 02912, USA.

M. Parente, Department of Electrical Engineering, Stanford University, Stanford, CA 94305, USA.